physica status solidi b
www.pss-b.com

Check for updates

Molecular Beam Epitaxy Growth and Characterization of Germanium-Doped Cubic $Al_xGa_{1-x}N$

Michael Deppe, Tobias Henksmeier, Jürgen W. Gerlach, Dirk Reuter, and Donat J. As*

In cubic (c-)GaN Ge has emerged as a promising alternative to Si for n-type doping, offering the advantage of slightly improved electrical properties. Herein, a study on Ge doping of the ternary alloy c-$Al_xGa_{1-x}N$ is presented. Ge-doped c-$Al_xGa_{1-x}N$ layers are grown by plasma-assisted molecular beam epitaxy. In two sample series, both the Al mole fraction x and the doping level are varied. The incorporation of Ge is verified by time-of-flight secondary ion mass spectrometry. Ge incorporation and donor concentrations rise exponentially with increasing Ge cell temperature. A maximum donor concentration of 1.4×10^{20} cm^{-3} is achieved. While the incorporation of Ge is almost independent of x, incorporation of O, which acts as an unintentional donor, increases for higher x. Dislocation densities start increasing when doping levels of around 3×10^{19} cm^{-3} are exceeded. Also photoluminescence intensities begin to drop at these high doping levels. Optical emission of layers with $x > 0.25$ is found to originate from a defect level 0.9 eV below the indirect bandgap, which is not related to Ge. In the investigated range $0 \leq x \leq 0.6$, Ge is a suitable donor in c-$Al_xGa_{1-x}N$ up to the low 10^{19} cm^{-3} range.

1. Introduction

In the recent past, much work has been done investigating Ge as an alternative n-type dopant in GaN. In Wurtzite GaN, the incorporation of Si, the most common donor for nitrides, leads to tensile strain.[1] This is not the case for incorporation of Ge; thus, the growth of highly doped layers with improved crystalline quality could be demonstrated.[2–4]

However, in GaN-based heterostructures grown in the Wurtzite crystal structure, the recombination efficiency can be impaired due to spontaneous and piezoelectric polarization fields. Growing the metastable cubic zinc blende phase is one way to overcome this effect as these fields are not present here.[5–8] The most common donor for cubic GaN (c-GaN) is Si, but recently, we have introduced Ge as an alternative n-type dopant for c-GaN.[9–11]

To extend the emission of nitride-based structures further into the ultraviolet spectral region, the ternary alloy $Al_xGa_{1-x}N$ can be grown. The most commonly used donor for Wurtzite and zinc blende $Al_xGa_{1-x}N$ is Si. Only a few experiments on Ge doping of Wurtzite $Al_xGa_{1-x}N$ have been reported in the past,[12] but recently detailed work on this topic has been published.[13,14] So far, no doping experiments with Ge for c-$Al_xGa_{1-x}N$ have been reported.

In this article, we introduce Ge as an n-type dopant for cubic $Al_xGa_{1-x}N$ grown by plasma-assisted molecular beam epitaxy (MBE) and report on the characterization results of doped layers with Al concentrations of $x \leq 0.6$.

2. Results and Discussion

The basic properties of the samples covered in this article are summarized in **Table 1**. Al mole fractions x were determined by two methods. The first one is to record the high-resolution X-ray diffraction (HRXRD) reciprocal space maps (RSMs)s around the asymmetric (113) reflections of the $Al_xGa_{1-x}N$ layers and calculate x from the layers' lattice constants. The second method is energy dispersive X-ray spectroscopy (EDX). The values obtained from both methods are in good agreement for each sample. Due to the higher accuracy, values measured by EDX are used to refer to the samples. Layer thicknesses were determined by reflectometric interference spectroscopy. In case of four samples from series 1 with a high x, the samples were too thin for accurate measurement (see annotation in Table 1). Instead, the estimated thickness based on the respective growth time and the average growth rate determined for the sample series ($\approx$105 nm h^{-1}) is given.

2.1. Growth Rate

In previous experiments,[9] we found that the growth rate of c-GaN is reduced by up to 40% when high Ge doping is applied, caused by an accumulation of Ge on the surface during growth. The reason for the accumulation is that during growth, a metal excess of one monolayer is maintained on the sample surface, which provides best conditions for c-GaN growth.[15] Due to

M. Deppe, T. Henksmeier, Prof. D. Reuter, Prof. D. J. As
Department of Physics
University of Paderborn
Warburger Str. 100, 33098 Paderborn, Germany
E-mail: michael.deppe@uni-paderborn.de

Dr. J. W. Gerlach
Non-thermal Deposition of Films and Structures
Leibniz Institute of Surface Engineering (IOM)
Permoserstr. 15, 04318 Leipzig, Germany

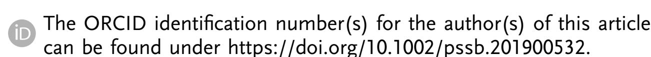
The ORCID identification number(s) for the author(s) of this article can be found under https://doi.org/10.1002/pssb.201900532.

© 2019 The Authors. Published by WILEY-VCH Verlag GmbH & Co. KGaA, Weinheim. This is an open access article under the terms of the Creative Commons Attribution License, which permits use, distribution and reproduction in any medium, provided the original work is properly cited.

DOI: 10.1002/pssb.201900532

 © 2019 The Authors. Published by WILEY-VCH Verlag GmbH & Co. KGaA, Weinheim

Table 1. Basic properties of the samples covered in this article.

Sample series	Al mole fraction x (EDX)	Al mole fraction x (HRXRD)	Ge temperature T_{Ge} [°C]	Ge Flux Φ [cm^{-2} s^{-1}]	Layer thickness d[a] [nm]	Donor concentration (CV) [cm^{-3}]	Dislocation density D (HRXRD) [cm^{-2}]
1	0	0	–	–	506	2.4×10^{17}	7.5×10^{9}
	0	0	800	2.9×10^{10}	427	1.4×10^{19}	1.0×10^{10}
	0.08	0.09	–	–	484	7.3×10^{17}	1.5×10^{10}
	0.09	0.10	800	2.9×10^{10}	480	9.6×10^{18}	1.6×10^{10}
	0.25	0.23	–	–	487	4.9×10^{18}	2.4×10^{10}
	0.24	0.26	800	2.9×10^{10}	456	1.6×10^{19}	3.0×10^{10}
	0.33	0.37	–	–	430	1.4×10^{19}	3.9×10^{10}
	0.39	0.38	800	2.9×10^{10}	336	2.5×10^{19}	5.0×10^{10}
	0.49	0.46	–	–	≈230[b]	1.8×10^{17}	4.7×10^{10}
	0.50	0.48	800	2.9×10^{10}	≈170[b]	1.9×10^{19}	4.9×10^{10}
	0.60	0.59	–	–	≈150[b]	1.8×10^{19}	–[c]
	0.63	0.62	800	2.9×10^{10}	≈140[b]	1.8×10^{19}	–[c]
2	0.23	0.23	–	–	497	4.2×10^{18}	2.5×10^{10}
	0.23	0.23	700	3.4×10^{8}	455	5.3×10^{18}	2.9×10^{10}
	0.26	0.27	800	2.9×10^{10}	437	1.5×10^{19}	3.1×10^{10}
	0.28	0.24	850	1.9×10^{11}	409	1.3×10^{19}	6.0×10^{10}
	0.26	0.22	900	9.3×10^{11}	438	7.5×10^{19}	6.5×10^{10}
	0.28	0.24	950	4.6×10^{12}	475	7.7×10^{19}	8.1×10^{10}
	0.22	0.22	1000	8.9×10^{12}	467	1.4×10^{20}	6.7×10^{10}

[a] measured by reflectometric interference spectroscopy; [b] too small for accurate measurement—estimated thickness based on growth rate and time; and [c] reflex overlapped by 3C-SiC substrate.

Table 2. Bond dissociation energies ΔH for different bonds containing Ge, Ga, Al, and N.

Bond	ΔH [kcal mol^{-1}]	Reference
Ge–N	61	[16]
	55	[17]
Ga–N	37.7	[18]
	48.5	[19]
Al–N	71.0	[20]
	63.5	[19]
Ge–Ge	45	[16]
	65.5	[21]
Ga–Ga	33.0	[21]
Al–Al	44.5	[20]

the higher dissociation energy of the Ge–Ge bond compared with the Ga–Ga bond (see **Table 2**), the evaporation of Ga from this excess layer is stronger than the evaporation of Ge, and an increasing amount of Ge can accumulate on the surface during growth. Impinging Ga atoms could be hindered by the Ge adlayer to reach the growth front. Furthermore, the Ge–N bond is more likely to be formed than the Ga–N bond. The dissociation energy of Al–N however is stronger than for Ge–N and Ga–N; thus, Al is directly built into the crystal, and no accumulation in the adlayer occurs for Al-containing layers. Growth rates of c-$Al_{0.25}Ga_{0.75}N$ layers grown at different Ge effusion cell temperatures T_{Ge} are shown in **Figure 1**. Within the accuracy limits—in contrast to layers containing no Al—no dependence of the growth rate on the Ge doping can be observed.

2.2. Structural Properties

To verify the incorporation of Ge into the layers, depth profiles of the layer compositions were measured by time-of-flight secondary ion mass spectrometry (TOF-SIMS). In **Figure 2**, the TOF-SIMS depth profile of the c-$Al_{0.25}Ga_{0.75}N$ layer grown at a $T_{Ge} = 900\,°C$ is shown exemplarily. The intensity of a selection of the recorded secondary ion signals is plotted versus the sputter time, which is proportional to the distance from the sample surface. After 770 s of sputtering, the 3C-SiC substrate is reached, resulting in a significant rise in the C^- and $^{29}Si^-$ signals. Measuring the $^{29}Si^-$ signal is preferred over $^{28}Si^-$, as the detector is not saturated due to the lower abundance of ^{29}Si. Within the c-$Al_{0.25}Ga_{0.75}N$ layer, the AlN^- and GaN^- signals run at a high intensity. Both Ge^- and GeN^- signals prove the incorporation of Ge into the layer. The intensity of the GeN^- signal is higher than the intensity of Ge^-, but the ratio between both signals depends on the Al mole fraction x. Furthermore, C^- and O^- signals are detected, which originate from impurities in the layer. C is known to form acceptors in c-GaN, and O is known to act as a donor.[22,23] All signals run stable within the c-$Al_{0.25}Ga_{0.75}N$ layer, indicating a high homogeneity of the layers. **Figure 3**a shows the

© 2019 The Authors. Published by WILEY-VCH Verlag GmbH & Co. KGaA, Weinheim

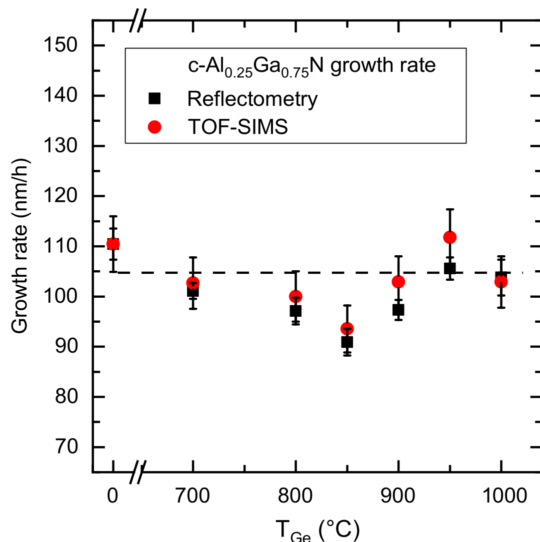

Figure 1. Growth rate of c-$Al_{0.25}Ga_{0.75}N$ layers for various Ge effusion cell temperatures T_{Ge}. Growth rates were calculated based on the layer thickness determined by reflectometric interference spectroscopy and the growth time (5 h). In addition, layer thicknesses were estimated from the TOF-SIMS sputter times that are required to reach the substrate, using the thickness of the NID layer measured by reflectometry as a reference. The mean growth rate is indicated by a dashed line (105 nm h^{-1}).

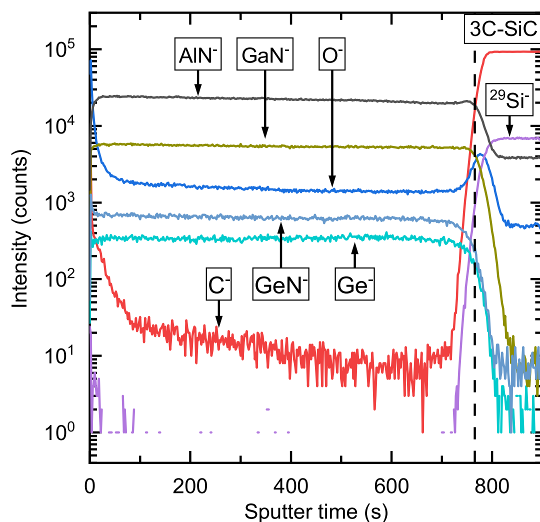

Figure 2. TOF-SIMS depth profile of a Ge-doped c-$Al_{0.25}Ga_{0.75}N$ layer (T_{Ge} = 900 °C). The dashed line indicates the interface between epilayer and 3C-SiC substrate.

Ge^- and O^- signal intensities as a function of x from samples with constant Ge doping (T_{Ge} = 800 °C, series 1). The Ge^- signal is nearly constant; it increases slightly with higher x. It is unclear if the incorporation of Ge is actually higher at higher x or if a SIMS-related matrix effect has to be considered. For the O^- signal, a linear increase is observed with increasing x both for Ge-doped and for not intentionally doped (NID) samples. The O^- signal at $x = 0.50$ is over six times higher than in the samples containing no Al. This corresponds to the observation by Kim et al.,[24] that Al favors the incorporation of O into GaN. Furthermore, the incorporation of impurities is enhanced by crystal defects,[25] and for samples with higher x, a slightly increased dislocation density is observed (see Table 1). The O^- signal from the NID sample with $x = 0.49$ deviates from the linear trend. The incorporation of O into this sample is significantly lower than expected. Since the growth conditions were comparable for all samples, there is no obvious reason for this behavior. In Figure 3b, the Ge^- and O^- signal intensities from c-$Al_{0.25}Ga_{0.75}N$ layers as a function of T_{Ge} are shown. An exponential dependency of the Ge^- signal on T_{Ge} is found, which in good approximation reflects the course of the Ge vapor pressure curve in this temperature range.[26] The O^- signal, on the other hand, exhibits a constant intensity over the entire range of T_{Ge}; hence, the unintentional incorporation of O is not affected by Ge doping.

To investigate the structural quality of the samples, atomic force microscopy (AFM) and HRXRD measurements were conducted. With AFM, a 5 × 5 μm^2 topographic image in the center of the sample is recorded and the root mean square roughness S_q is calculated. In **Figure 4**, the S_q values are plotted versus T_{Ge} for the c-$Al_{0.25}Ga_{0.75}N$ samples. Average values between 3 and 6 nm are obtained, except for two samples: a minimum roughness of 1.9 nm is measured for T_{Ge} = 800 °C (**Figure 5**a) and a considerable increase above 11 nm occurs for the highest doping at T_{Ge} = 1000 °C (Figure 5b). The surface of this sample is characterized by droplets and line-shaped hills, which probably are deposits of the metal elements. It seems that in general light Ge doping results in a smoother surface, whereas high Ge concentrations lead again to an increased surface roughness. **Figure 6** shows the roughness of the NID and Ge-doped (T_{Ge} = 800 °C) samples with varying x. One has to consider that the layers of this series are not of equal thickness. With greater thickness also the roughness becomes higher. Nevertheless, it is obvious that with supply of Ge (at least at T_{Ge} = 800 °C) smoothing of the surface occurs.

HRXRD rocking curves of the (002) reflexes were measured to obtain the dislocation density of the layers. The dislocation density D can be estimated by[27]

$$D = \frac{\Delta\theta^2}{9b^2} \quad (1)$$

where $\Delta\theta$ is the full width at half maximum (FWHM) of the rocking curve and b is the length of the Burgers vector. For 60° dislocations, the length of the Burgers vector is[28]

$$b = \frac{a}{\sqrt{2}} \quad (2)$$

where a is the lattice constant of c-$Al_xGa_{1-x}N$ according to Vegard's rule linearly interpolated between $a_{c\text{-}GaN}$ = 4.503 Å[29] and $a_{c\text{-}AlN}$ = 4.373 Å.[30] Up to T_{Ge} = 800 °C, the dislocation density is nearly constant at around 3 × 10^{10} cm^{-2} but is doubled at higher doping. According to the capacitance–voltage (CV) measurements (see Section 2.3), the dislocation density begins to rise in the low 10^{19} cm^{-3} doping range. By means of RSMs around the (002) reflections, the purity of the cubic phase can be evaluated. Hexagonal inclusions in c-GaN mainly grow on (111) facets,[8] and their $(\bar{1}011)$ and $(10\bar{1}1)$ reflections appear in the vicinity

© 2019 The Authors. Published by WILEY-VCH Verlag GmbH & Co. KGaA, Weinheim

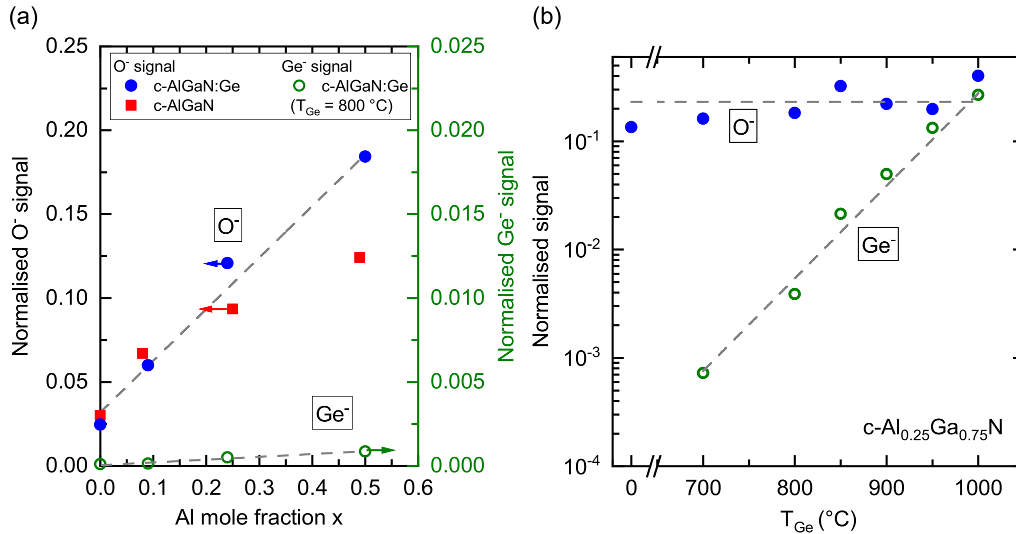

Figure 3. a) Signals from O^- and Ge^- ions measured by TOF-SIMS for NID and Ge-doped ($T_{Ge} = 800\,°C$) c-$Al_xGa_{1-x}N$ layers. The incorporation of O rises linearly with increasing Al mole fraction x, whereas the Ge^- signal is nearly constant. b) O^- and Ge^- signals from c-$Al_{0.25}Ga_{0.75}N$ layers with varying T_{Ge}. The Ge^- signal rises exponentially with increasing T_{Ge}, the incorporation of O however is not affected by T_{Ge}. In both diagrams, the signals are normalized to the $^{29}Si^-$ signals in the 3C-SiC substrate to account for varying sputter conditions. Please note that the y-scale is linear in (a) and logarithmic in (b).

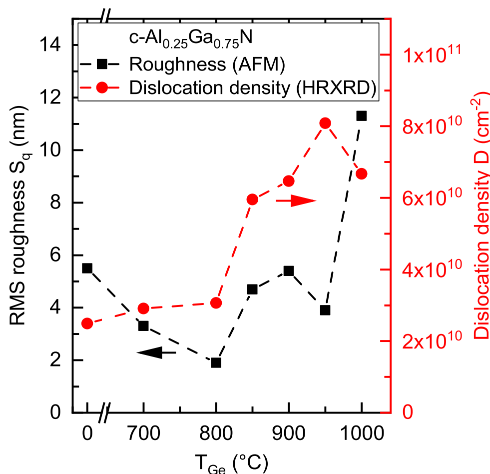

Figure 4. Roughness measured by AFM in $5 \times 5\,\mu m^2$ (left scale, squares) and dislocation density estimated from HRXRD (right scale, circles) of c-$Al_{0.25}Ga_{0.75}N$ layers depending on the Ge effusion cell temperature T_{Ge}.

of the cubic (002) reflection.[8,31] Up to $T_{Ge} = 850\,°C$, no hexagonal inclusions are apparent in the RSMs. With further increased doping, however, the intensities of hexagonal inclusions add up to around 10% of the respective cubic reflection's intensity. It is also notable that the reflection high-energy electron diffraction (RHEED) pattern of the highest doped sample ($T_{Ge} = 1000\,°C$) indicates the formation of a polycrystalline phase, which is not the case for all of the other samples. Regarding the sample series with fixed $T_{Ge} = 800\,°C$ and varying x in general, no significant difference can be found concerning the dislocation density and the amount of hexagonal inclusions between doped and NID samples.

2.3. Electrical Characterization

CV spectroscopy was performed to obtain the donor concentration in the c-$Al_xGa_{1-x}N$ layers. For this purpose, both a gate contact and an ohmic contact are required. To prepare the gates, circular Au contacts with diameters from 200 to 800 μm were deposited on 100 nm-thick SiO_2 acting as a gate isolation. To achieve ohmic contacts, In was alloyed onto the sample corners. An alternating current (AC) signal ($f = 1$ MHz) of 5 mV was superimposed to a sweeping direct current (DC) voltage V_g from −1 to +4 V, and the capacitance C is measured by an LCR (inductance L, capacitance C, and resistance R) meter. With the gate area S, the donor concentration N_D is calculated by[32]

$$N_D = \frac{2}{e\varepsilon_s\varepsilon_0 S^2}\left(\frac{dC_s^{-2}}{dV_g}\right). \tag{3}$$

In **Figure** 7a, the donor concentrations N_D for the sample series with varying x are shown (series 1). The donor concentration in the NID samples rises almost linearly with increasing x from $2.4 \times 10^{17}\,cm^{-3}$ at $x = 0$ up to $1.8 \times 10^{19}\,cm^{-3}$ at $x = 0.60$ (red squares and red linear fit curve). This increase in unintentional doping is assigned to the incorporation of O during growth. In the TOF-SIMS measurements (cf. Figure 3a), the amount of O also shows a linear dependence on x. Interestingly, the measured donor concentration of the NID sample with $x = 0.49$, which exhibited an unexpectedly low O^- signal in the TOF-SIMS measurements, also deviates downward from the linear fit to the CV results. The reason for the deviation of this data point from the linear behavior has been unclear up to now; however, the similar behavior additionally supports the fact that O may be the origin of the unintentional background doping. The donor concentration in Ge-doped layers (at $T_{Ge} = 800\,°C$) is nearly

© 2019 The Authors. Published by WILEY-VCH Verlag GmbH & Co. KGaA, Weinheim

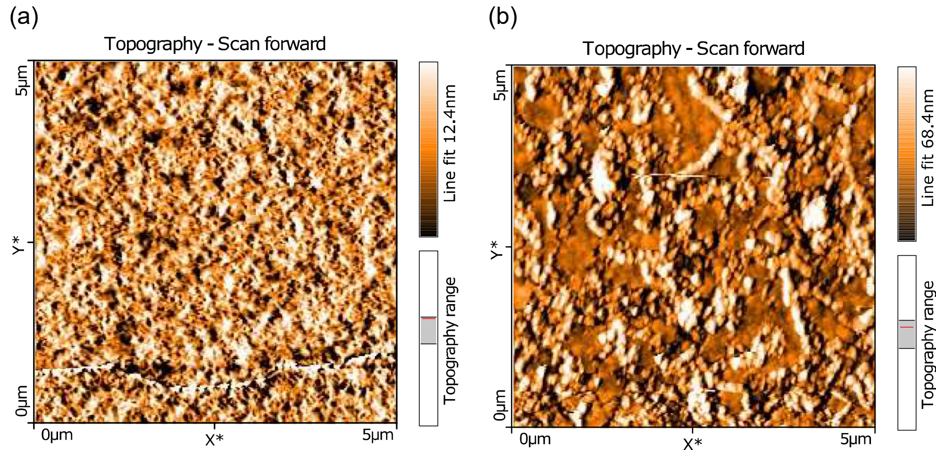

Figure 5. Surface topography of c-$Al_{0.25}Ga_{0.75}N$ layers measured by AFM. The Ge effusion cell temperature for the sample in (a) was $T_{Ge} = 800\,°C$ and a root mean square roughness of $S_q = 1.9$ nm is measured. For (b) $T_{Ge} = 1000\,°C$ and a roughness of $S_q = 11.3$ nm is measured.

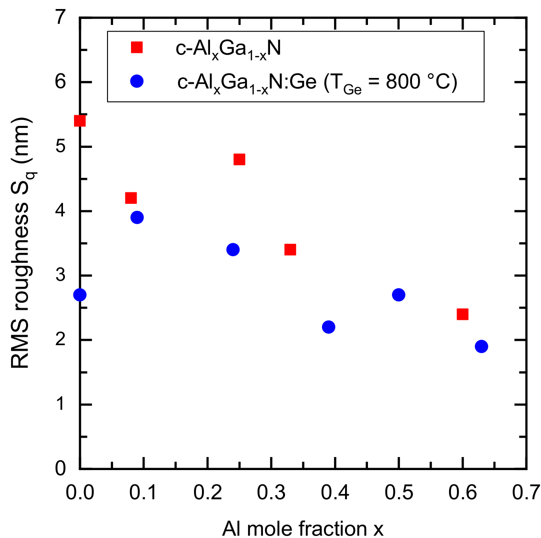

Figure 6. Roughness measured by AFM of NID and Ge-doped ($T_{Ge} = 800\,°C$) c-$Al_xGa_{1-x}N$ layers. Please note that layers with a higher x have lower thicknesses and thus in general feature smoother surfaces.

independent of x; it is slightly increasing with a higher Al content and ranges at about 1–2 × 10^{19} cm^{-3} This observation agrees with the fact that the Ge^- concentration measured by TOF-SIMS is nearly constant over the investigated range of x. In addition to CV spectroscopy, we have exemplarily conducted Hall effect measurements at room temperature in van der Pauw geometry for the two samples with $x \approx 0.1$. Both samples exhibit n-type conductivity. Free electron concentrations of 7.7 × 10^{17} and 5.4 × 10^{18} cm^{-3} are measured for the NID sample and the doped sample ($T_{Ge} = 800\,°C$), respectively. These values are in good agreement with the values obtained by CV spectroscopy.

The dependence of the donor concentrations on T_{Ge} measured by CV spectroscopy for c-$Al_{0.25}Ga_{0.75}N$ (series 2) is shown in Figure 7b. Like the Ge^- signal from TOF-SIMS measurements (cf. Figure 3b), the donor concentration rises exponentially with increasing T_{Ge}, resembling the course of the vapor pressure curve of Ge. A maximum donor concentration of 1.4 × 10^{20} cm^{-3} is achieved at $T_{Ge} = 1000\,°C$. However, as shown in Section 2.2, the structural quality of this sample is poor. The dislocation density does not rise for Ge cell temperatures up to 800 °C, which corresponds to a donor concentration of 1.5 × 10^{19} cm^{-3}. Therefore, considering the structural degradation, the maximum reasonably achievable donor concentration in c-$Al_{0.25}Ga_{0.75}N$ is approximately one order of magnitude lower than in c-GaN.[9,11]

2.4. Photoluminescence Spectroscopy

Figure 8a shows the photoluminescence (PL) spectra of NID and Ge-doped c-GaN samples (i.e., without Al, $x = 0$). The near-band-edge emission of the NID sample mainly consists of three peaks. The emission at 3.262 eV originates from the recombination of donor-bound excitons (D^0,X).[33] The peak at 3.137 eV is assigned to a donor–acceptor pair recombination (D^0,A^0).[33] At 3.068 eV, an additional donor–acceptor pair recombination can be observed; we assume C to be involved as an acceptor.[22,34] With Ge doping at $T_{Ge} = 800\,°C$, a distinct change in PL spectrum can be observed. The overall emission intensity rises strongly. The intensity of the (D^0,A^0) peak is higher by a factor of 10 in the doped sample compared with the NID sample. Furthermore, the intensity of the (D^0,A^0) transition becomes more intense in relation to (D^0,X). While the energy of the (D^0,X) transition remains unchanged (indicated by the dashed line), the (D^0,A^0) peak shifts by 52 meV to 3.189 eV due to Coulomb interaction between donors and acceptors.[10] The Coulomb interaction energy is given by[35]

$$\Delta E = \frac{e^2}{4\pi\varepsilon_0\varepsilon_r r} \tag{4}$$

where $\varepsilon_r = 9.44$ is the relative permittivity of c-GaN[36] and r the mean distance from acceptors to donors[36]

$$r = \sqrt[3]{\frac{3}{4\pi N_{Ge}}} \tag{5}$$

© 2019 The Authors. Published by WILEY-VCH Verlag GmbH & Co. KGaA, Weinheim

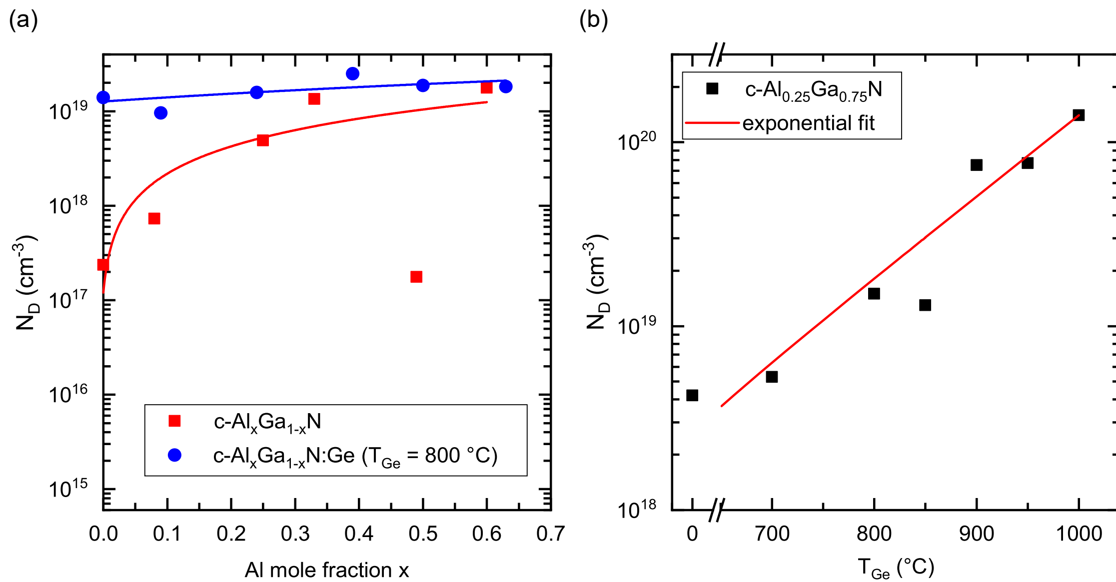

Figure 7. a) Donor concentration versus Al mole fraction x measured by CV spectroscopy for NID (squares) and Ge-doped layers ($T_{Ge} = 800\,°C$, dots). Linear functions are fitted to the data points. The donor concentration in NID samples rises linearly with increasing Al mole fraction. In Ge-doped samples, the donor concentration is nearly constant over the investigated range of x. b) Donor concentrations measured by CV spectroscopy for fixed $x = 0.25$ and varying Ge effusion cell temperature T_{Ge}. In the investigated temperature range, the donor concentration rises exponentially with increasing cell temperature. The maximum achieved donor concentration is $1.4 \times 10^{20}\,cm^{-3}$.

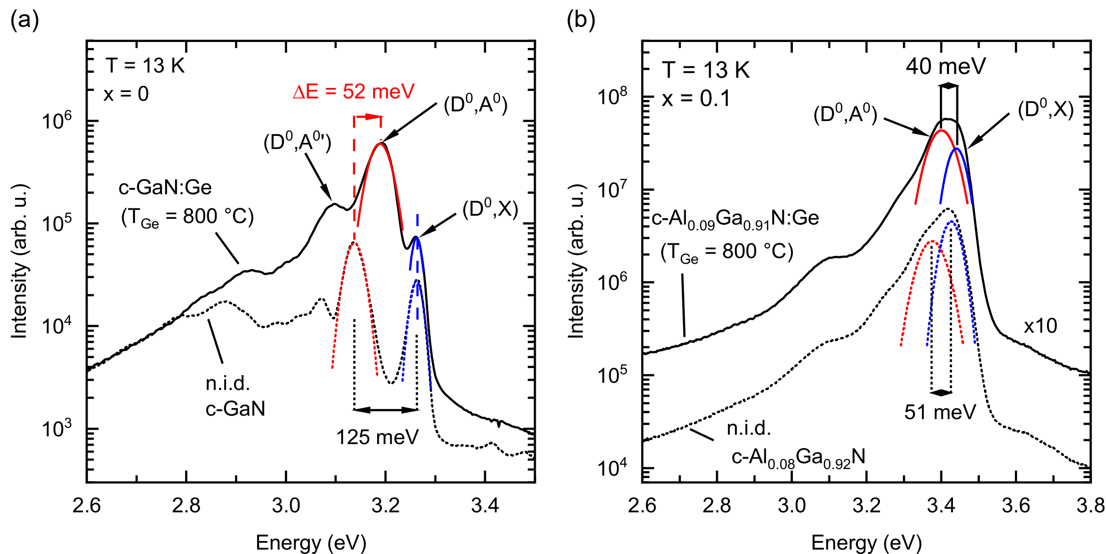

Figure 8. a) PL spectra at 13 K of the NID (dotted) and Ge-doped (solid) c-GaN samples. Multipeak fits were performed to obtain the peak energies. b) PL spectra at 13 K of the NID (dotted) and Ge-doped (solid) c-$Al_{0.1}Ga_{0.9}N$ samples. For better clarity, the spectrum of the doped sample is shifted vertically by a factor of 10, as the emission intensities of both samples are nearly identical. Multipeak fits were performed to illustrate the composition of the near band-edge emission and obtain the peak energies.

From these relations, a donor concentration of $N_{Ge} = 4 \times 10^{18}\,cm^{-3}$ is estimated for the Ge-doped ($T_{Ge} = 800\,°C$) c-GaN sample, which is consistent with the actual Ge concentration $N_{Ge} = 6.0 \times 10^{18}\,cm^{-3}$ determined by TOF-SIMS.[11]

In Figure 8b, the PL spectra of the doped ($T_{Ge} = 800\,°C$) and NID samples with $x \approx 0.1$ are shown. The emission intensities of both samples are nearly identical. The separate emission peaks which could be observed in the samples without Al have now merged to a broad emission and have shifted to higher energies due to the increased bandgap energy of $Al_{0.1}Ga_{0.9}N$. By performing multipeak fits, it becomes clear that this broad emission is composed of two emission peaks, which are expected to stem from the same processes as observed for c-GaN, namely an

© 2019 The Authors. Published by WILEY-VCH Verlag GmbH & Co. KGaA, Weinheim

excitonic recombination (D^0,X) and a donor–acceptor pair recombination (D^0,A^0). The (D^0,X) peak in the NID sample is located at 3.426 eV; in the Ge-doped sample, it is found at 3.440 eV. This difference is in agreement with the deviating bandgap s in both samples due to the slightly different Al content x (see Table 1). In the NID sample, the (D^0,A^0) peak is found at 3.375 eV, which is 51 meV below the (D^0,X) transition. For comparison, the difference between (D^0,X) and (D^0,A^0) in the NID sample without Al is 125 meV (see Figure 8a). This means that the (D^0,A^0) transition in the NID c-$Al_{0.09}Ga_{0.91}N$ sample underwent a blueshift of 74 meV compared with the c-GaN sample, which is ascribed to the Coulomb interaction caused by the unintentional O doping. In the Ge-doped c-$Al_{0.10}Ga_{0.90}N$ sample the difference between the (D^0,X) and (D^0,A^0) transition is further reduced to 40 meV. Therefore, a stronger Coulomb interaction occurs due to additional Ge doping. Like in the case of the c-GaN samples, with increased doping, the (D^0,A^0) emission intensity becomes stronger at the expense of the intensity of the (D^0,X) transition.

In **Figure 9**, the 13 K PL spectra of doped ($T_{Ge} = 800\,°C$, full curves) and NID layers (dotted curves) with different Al mole fractions x are shown over an extended spectral range between 2.35 and 4.6 eV (series 1). The spectra are normalized to the peak emission and shifted vertically for better clarity. The direct bandgaps for the corresponding cubic $Al_xGa_{1-x}N$ samples are indicated by arrows. These energy gap values were estimated by ellipsometric measurements and theoretical calculations.[37] With increasing x, the spectra shift to higher energies and become broader. Above an Al content of $x \geq 0.2$, the increased background doping by O and the broadening of the emission band due to alloying result in a merge of the exciton band and the donor–acceptor band. Therefore, no reasonable multipeak fit could be performed anymore to separate the different transitions unlike in the case of samples with $x \leq 0.1$ (see above). As shown in Figure 7a, in the NID $Al_xGa_{1-x}N$ layers, the carrier concentration N_D due to background doping becomes comparable with the carrier concentration incorporated by the Ge-doped samples. Therefore, no difference in the PL spectra of the NID and the Ge-doped samples is expected for the samples with a higher Al content. Further careful analysis of the spectra shows that at higher Al concentrations, the peaks of the spectra increasingly deviate from the estimated bandgap energy (arrows), indicating that an additional deep emission band becomes dominant at high x.

To further investigate the origin of the dominant emission in samples with $x > 0.2$, the peak energies of the dominant emission are plotted versus x in **Figure 10**. In addition, the low-temperature direct and indirect bandgaps of c-$Al_xGa_{1-x}N$[37] are shown in the diagram. Up to $x = 0.1$, the emission follows the direct bandgap in excellent agreement. At $x \geq 0.37$, however, the emission energies follow a deep defect energy level that lies 0.9 eV below the indirect bandgap of c-$Al_xGa_{1-x}N$. The emission of the samples with $x = 0.23$ and $x = 0.26$ is neither related to the bandgap, nor to the deep defect level. The crossover of the direct bandgap and the deep defect level occurs at $x \approx 0.25$.

Currently, the origin of this deep defect level is unclear and demands additional investigation. One possibility is that a DX center is formed by O. In Wurtzite, $Al_xGa_{1-x}N$ with $x > 0.3$ O is known to form DX centers,[23,38,39] but theoretical calculations suggest that no DX formation occurs in the cubic phase.[38]

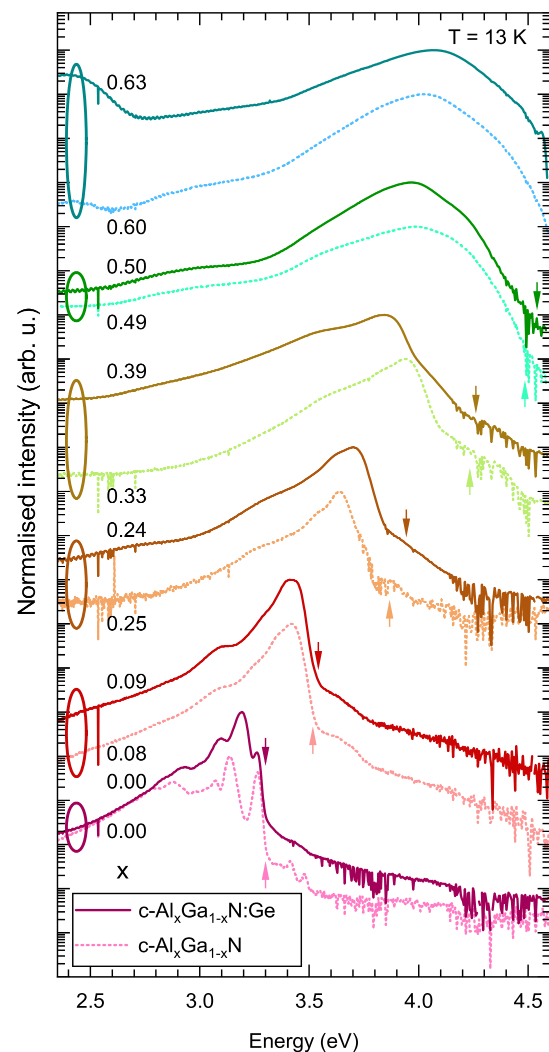

Figure 9. PL spectra of Ge-doped ($T_{Ge} = 800\,°C$, full curves) and NID (dotted curves) $Al_xGa_{1-x}N$ layers taken at 13 K. Spectra are normalized to the peak emission and shifted vertically for better clarity. The numbers besides the spectra denote the Al mole fractions x. Dotted spectra belong to NID samples and Ge-doped spectra are drawn with solid lines. Arrows indicate the direct bandgaps for the respective Al mole fraction.[37]

Due to the fact that the emission of both the NID samples and the Ge-doped samples sticks to the same energy level at $x > 0.25$, the deep defect level seems not to be related to the incorporation of Ge.

In **Figure 11**a, the normalized 13 K PL spectra of c-$Al_{0.25}Ga_{0.75}N$ layers grown with varying T_{Ge} (series 2) are shown. The spectra are shifted vertically for better clarity. Up to $T_{Ge} = 800\,°C$, the main emission band lies below the bandgap $E_g \approx 3.92$ eV[37] (discussed earlier) and consists of two emission peaks. It seems reasonable to assume that these peaks originate from donor-bound excitons (D^0,X) and a donor–acceptor pair recombination (D^0,A^0) (see earlier sections and Figure 8). The (D^0,A^0) peak at the low-energy shoulder of the main emission band rises in intensity to the disadvantage of the (D^0,X) peak when doping is increased up to $1.5 \times 10^{19}\,cm^{-3}$

© 2019 The Authors. Published by WILEY-VCH Verlag GmbH & Co. KGaA, Weinheim

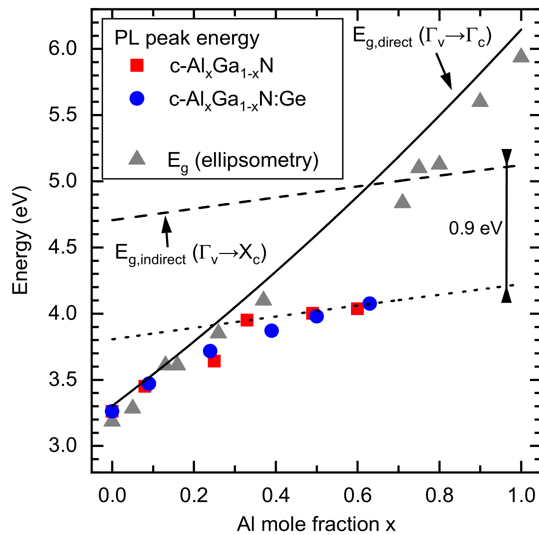

Figure 10. Peak energy of the 13 K PL of NID (squares) and Ge-doped (dots) samples depending on the Al mole fraction x. The low-temperature direct and indirect bandgaps of c-Al$_x$Ga$_{1-x}$N[37] are shown by solid and dashed lines, respectively. The dotted line represents the indirect bandgap reduced by 0.9 eV. Triangles indicate the bandgap experimentally determined by ellipsometry at 300 K.[37] The difference to the solid line is due to the thermal shift of the bandgap.

($T_{Ge} = 800\,°C$). With further increasing T_{Ge}, the spectra become broader and shift to higher energies. The peak emission at $T_{Ge} = 950\,°C$ lies above the bandgap, probably due to the Moss–Burstein effect,[40,41] indicating degenerate doping. The integral intensities of the spectra are plotted versus T_{Ge} in Figure 11b. Intensities increase by over one order of magnitude with medium doping compared with the NID layer but begin to drop above $T_{Ge} = 850\,°C$. This effect indicates that nonradiative recombination centers are formed when high Ge fluxes are incorporated into the layers. Also, the dislocation density is significantly increased at $T_{Ge} \geq 850\,°C$ (cf. section 2.2), which reduces the radiative efficiency. The PL intensity of the highest doped sample is almost four orders of magnitude lower than that of the samples grown at $T_{Ge} = 700\,°C$ and $T_{Ge} = 800\,°C$. Comparing with the CV measurements (Section 2.3) shows that the PL intensity begins to drop when doping exceeds the low $10^{19}\,cm^{-3}$ doping range.

3. Conclusion

We have investigated Ge as an n-type dopant in c-Al$_x$Ga$_{1-x}$N layers grown by MBE. Layers with Al mole fractions x between 0 and 0.6 were grown with fixed Ge doping ($N_{Ge} \approx 10^{19}\,cm^{-3}$) and no intentional doping, and c-Al$_{0.25}$Ga$_{0.75}$N layers were grown with varying donor concentrations up to $N_{Ge} \approx 10^{20}\,cm^{-3}$. While the growth rate of c-GaN is reduced at high Ge fluxes, no reduction in the growth rate is observed when growing doped layers containing Al. The incorporation of Ge into all doped layers is verified by TOF-SIMS. The Ge concentration measured by TOF-SIMS and the donor concentration measured by CV spectroscopy both increase proportionally to the Ge vapor pressure curve. A maximum donor concentration of $1.4 \times 10^{20}\,cm^{-3}$ in c-Al$_{0.25}$Ga$_{0.75}$N is measured by CV spectroscopy. By means of TOF-SIMS, it is also found that a higher Al mole fraction x favors the unintentional incorporation of O, which also acts as an n-type dopant in c-Al$_x$Ga$_{1-x}$N. Dislocation densities of the layers were evaluated using HRXRD. Structural degradation of c-Al$_{0.25}$Ga$_{0.75}$N layers doped higher than $\approx 3 \times 10^{19}\,cm^{-3}$ was observed. PL spectroscopy revealed clearly separable emission peaks for doped and undoped c-GaN. The emission peaks merge to a broad emission band as x increases. We assume a high doping level even in NID Al-containing samples due to unintentional incorporation of O. For small x, the near-band-edge emission follows the direct bandgap of c-Al$_x$Ga$_{1-x}$N. Above a crossover point

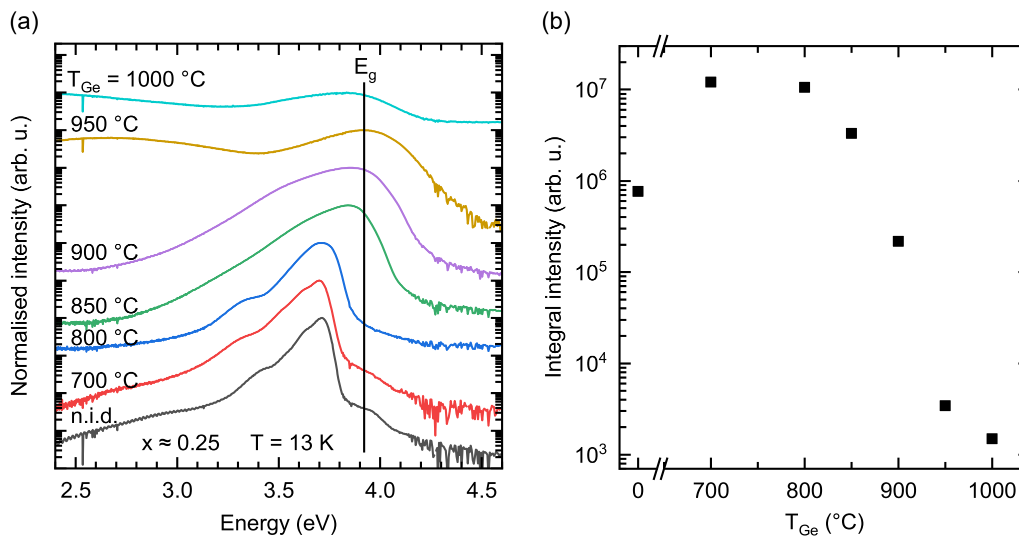

Figure 11. a) PL spectra of c-Al$_{0.25}$Ga$_{0.75}$N layers recorded at 13 K. Spectra are normalized to the peak emission and shifted vertically for better clarity. The bandgap of c-Al$_{0.25}$Ga$_{0.75}$N at 13 K is visualized by the solid line ($E_g \approx 3.92$ eV).[37] b) Integral intensity of the c-Al$_{0.25}$Ga$_{0.75}$N PL spectra at 13 K depending on the Ge effusion cell temperature T_{Ge}.

© 2019 The Authors. Published by WILEY-VCH Verlag GmbH & Co. KGaA, Weinheim

of $x = 0.25$, the emission is related to a deep defect level which lies 0.9 eV below the indirect bandgap but is very likely not caused by Ge doping. For the c-$Al_{0.25}Ga_{0.75}N$ sample series, we find an increasing PL intensity when doping is increased up to the low 10^{19} cm^{-3} range, but intensities drop with further increased doping. Overall, Ge is suited for n-type doping of c-$Al_xGa_{1-x}N$ within the investigated range of parameters. Considering the structural degradation at very high doping, the maximum reasonably achievable doping level in c-$Al_{0.25}G_{0.75}N$ is around 3×10^{19} cm^{-3}.

4. Experimental Section

The cubic (c-)$Al_xGa_{1-x}N$ layers examined in this article were grown by plasma-assisted MBE in a Riber-32 system. Activated N atoms were supplied by an Oxford Applied Research HD25 radio frequency plasma source. A total of 10 μm 3C-SiC (001) layers deposited on 500 μm Si (001) were used as substrates. Two different series of c-$Al_xGa_{1-x}N$ layers were grown. In the first series, the Al mole fraction x was varied between 0 and 0.6, as c-$Al_xGa_{1-x}N$ becomes indirect for x between 0.64 and 0.71.[37] For each x, an NID and a Ge-doped layer was grown. For doped samples, a Ge effusion cell temperature of 800 °C was chosen to achieve a donor concentration in the order of 10^{19} cm^{-3}. In the second series, x was kept constant at 0.25, and the Ge effusion cell temperature was varied from 700 to 1000 °C, resulting in donor concentrations of up to 1.4×10^{20} cm^{-3}. The N_2 flow ranged between 0.18 and 0.21 sccm, and the plasma source was operated at a power of 260 W. The Al beam equivalent pressure (BEP) was adjusted to the respective fraction x of the BEP required for pure c-AlN growth, which is 6.9×10^{-8} mbar. The Ga BEP was then adjusted such that slightly metal-rich growth conditions with a total metal excess of one monolayer were achieved. The growth process—especially the adjustment of the metal excess monolayer[15]—was monitored in situ using RHEED. For layers of the first series, a growth time of 4.5 h was set. However, at a higher x, eventually evidence of hexagonal inclusions became visible in the RHEED patterns; thus, the growth was stopped at that point. The growth time for all samples of the second series was 5 h.

The actual Al mole fraction x of the samples was determined by HRXRD on a Philips X'Pert MRD by measuring RSMs around the asymmetric (113) reflexes and by EDX using an EDAX EDX system with a Si drift detector equipped to a JEOL JSM-6060 scanning electron microscope. HRXRD rocking curves of the (002) reflexes were taken to estimate the dislocation densities of the layers and RSMs around the (002) reflexes were measured to evaluate the amount of hexagonal inclusions in our layers. PL spectroscopy was conducted using a CryLaS FQCW-266 continuous wave frequency-quadrupled Nd:YAG laser emitting at 266 nm with a power of 5 mW as an excitation source. For light detection, an Andor iDus 420 CCD equipped to a SPEX 270M imaging spectrograph was used. The layer thickness of each sample was measured by reflectometric interference spectroscopy. TOF-SIMS was used by an ION-TOF TOF-SIMS 5 instrument to gain depth-resolved insight into the composition of the layers. Therefore, a primary ion beam of 15 keV $^{69}Ga^+$ ions scanned a 50×50 μm^2 area for analysis. A Cs^+ beam covering a 300×300 μm^2 area was taken for depth profiling. AFM was performed using a Nanosurf Mobile S atomic force microscope operating in contact mode to investigate the surface topography. CV spectroscopy was applied to determine the donor concentration in our layers, utilizing an Agilent E4980A LCR meter.

Acknowledgements

The authors would like to thank Fabian Tacken for the preparation of a part of the samples. This work was financially supported by the Deutsche Forschungsgemeinschaft (DFG, German Research Foundation)—Projektnummer 231447078—TRR 142 (via project B02).

Conflict of Interest

The authors declare no conflict of interest.

Keywords

AlGaN, doping, germanium, molecular beam epitaxy

Received: August 30, 2019
Revised: October 17, 2019
Published online: November 4, 2019

[1] L. T. Romano, C. G. Van de Walle, B. S. Krusor, R. Lau, J. Ho, T. Schmidt, J. W. Ager III, W. Götz, R. S. Kern, *Physica B* **1999**, *273–274*, 50.
[2] S. Fritze, A. Dadgar, H. Witte, M. Bügler, A. Rohrbeck, J. Bläsing, A. Hoffmann, A. Krost, *Appl. Phys. Lett.* **2012**, *100*, 122104.
[3] A. Dadgar, J. Bläsing, A. Diez, A. Krost, *Appl. Phys. Express* **2011**, *4*, 011001.
[4] M. N. Fireman, G. L'Heureux, F. Wu, T. Mates, E. C. Young, J. S. Speck, *J. Cryst. Growth* **2019**, *508*, 19.
[5] D. Schikora, D. J. As, K. Lischka, in *Vacuum Science and Technology: Nitrides as Seen by the Technology* (Eds: T. Paskova, B. Monemar), Research Signpost, Kerala, India **2002**, Ch. 15.
[6] D. J. As, *III-Nitride Semiconductor Growth* (Eds: M. O. Manasreh, I. T. Ferguson), Taylor & Francis, New York **2003**, Ch. 9.
[7] D. J. As, *Microelectron. J.* **2009**, *40*, 204.
[8] D. J. As, K. Lischka, in *Molecular Beam Epitaxy: From Research to Mass Production* (Ed: M. Henini), Elsevier, Amsterdam **2013**, p. 206.
[9] M. Deppe, J. W. Gerlach, D. Reuter, D. J. As, *Phys. Status Solidi B* **2017**, *254*, 1600700.
[10] D. J. As, M. Deppe, J. W. Gerlach, D. Reuter, *MRS Adv.* **2017**, *2*, 283.
[11] M. Deppe, J. W. Gerlach, S. Shvarkov, D. Rogalla, H.-W. Becker, D. Reuter, D. J. As, *J. Appl. Phys.* **2019**, *125*, 095703.
[12] X. Zhang, P. Kung, A. Saxler, D. Walker, T. C. Wang, M. Razeghi, *Appl. Phys. Lett.* **1995**, *67*, 1745.
[13] R. Blasco, A. Ajay, E. Robin, C. Bougerol, K. Lorentz, L. C. Alves, I. Mouton, L. Amichi, A. Grenier, E. Monroy, *J. Phys. D: Appl. Phys.* **2019**, *52*, 125101.
[14] A. Bansal, K. Wang, J. S. Lundh, S. Choi, J. M. Redwing, *Appl. Phys. Lett.* **2019**, *114*, 142101.
[15] J. Schörmann, S. Potthast, D. J. As, K. Lischka, *Appl. Phys. Lett.* **2007**, *90*, 041918.
[16] D. A. Johnson, *Some Thermodynamic Aspects of Inorganic Chemistry*, Cambridge University Press, Cambridge **1976**, p. 159.
[17] F. P. Pruchnik, *Organometallic Chemistry of the Transition Elements*, Springer, New York **1990**, p. 202.
[18] S. Porowski, I. Grzegory, in *Properties of Group III Nitrides* (Ed: J. H. Edgar), INSPEC, London **1994**, p. 76.
[19] H. Morkoç, *Handbook of Nitride Semiconductors and Devices*, Vol. *1*, Wiley-VCH, Weinheim **2008**, p. 6.
[20] J. A. Dean, *Lange's Handbook of Chemistry*, 15th ed., McGraw-Hill, New York **1999**, p. 4.41.
[21] J. A. Dean, *Lange's Handbook of Chemistry*, 15th ed., McGraw-Hill, New York **1999**, p. 4.45.
[22] D. J. As, *Defect Diffus. Forum* **2002**, *206–207*, 87.
[23] C. G. Van de Walle, J. Neugebauer, *J. Appl. Phys.* **2004**, *95*, 3851.
[24] H. Kim, F. J. Fälth, T. G. Andersson, *J. Electron. Mater.* **2001**, *30*, 1343.

© 2019 The Authors. Published by WILEY-VCH Verlag GmbH & Co. KGaA, Weinheim

[25] G. Popovici, W. Kim, A. Botchkarev, H. Tang, H. Morkoç, J. Solomon, *Appl. Phys. Lett.* **1997**, *71*, 3385.
[26] *Landolt-Börnstein, Group III*, Vol. *41*, Subvol. A1b (Eds: O. Madelung, U. Rössler, M. Schulz), Springer-Verlag, Berlin **2002**, Online Document 533, p. 1.
[27] P. Gay, P. B. Hirsch, A. Kelly, *Acta Metall.* **1953**, *1*, 315.
[28] A. T. Blumenau, J. Elsner, R. Jones, M. I. Heggie, S. Öberg, T. Frauenheim, P. R. Briddon, *J. Phys.: Condens. Matter* **2000**, *12*, 10223.
[29] I. Akasaki, H. Amano, in *Properties of Group III Nitrides* (Ed: J. H. Edgar), INSPEC, London **1994**, p. 30.
[30] T. Schupp, K. Lischka, D. J. As, *J. Cryst. Growth* **2010**, *312*, 1500.
[31] Z. X. Qin, H. Nagano, Y. Sugure, A. W. Jia, M. Kobayashi, Y. Kato, A. Yoshikawa, K. Takahashi, *J. Cryst. Growth* **1998**, *189/190*, 425.
[32] N. Arora, *MOSFET Modeling For VLSI Simulation*, World Scientific, Singapore **2007**.
[33] D. J. As, F. Schmilgus, C. Wang, B. Schöttker, D. Schikora, K. Lischka, *Appl. Phys. Lett.* **1997**, *70*, 1311.
[34] D. J. As, U. Köhler, M. Lübbers, J. Mimkes, K. Lischka, *Phys. Status Solidi A* **2001**, *188*, 699.
[35] D. K. Schroder, *Semiconductor Material and Device Characterization*, John Wiley & Sons, Inc., Hoboken, New Jersey **2006**, p. 606.
[36] M. Feneberg, M. Röppischer, C. Cobet, N. Esser, J. Schörmann, T. Schupp, D. J. As, F. Hörich, J. Bläsing, A. Krost, R. Goldhahn, *Phys. Rev. B* **2012**, *85*, 155207.
[37] M. Landmann, E. Rauls, W. G. Schmidt, M. Röppischer, C. Cobet, N. Esser, T. Schupp, D. J. As, M. Feneberg, R. Goldhahn, *Phys. Rev. B* **2013**, *87*, 195210.
[38] C. G. Van de Walle, *Phys. Rev. B* **1998**, *57*, R2033.
[39] M. D. McCluskey, N. M. Johnson, C. G. Van de Walle, D. P. Bour, M. Kneissl, W. Walukiewicz, *Phys. Rev. Lett.* **1998**, *80*, 4008.
[40] E. Burstein, *Phys. Rev.* **1954**, *93*, 632.
[41] T. S. Moss, *Proc. Phys. Soc. B* **1954**, *67*, 775.

© 2019 The Authors. Published by WILEY-VCH Verlag GmbH & Co. KGaA, Weinheim